J|A|C|S
ARTICLES
Published on Web 11/26/2003

Nitrogen Binding to the FeMo-Cofactor of Nitrogenase

Johannes Schimpl,[†] Helena M. Petrilli,[‡] and Peter E. Blöchl*,[†]

Contribution from the Institute for Theoretical Physics, Clausthal University of Technology, D-38678 Clausthal-Zellerfeld, Germany, and Instituto de Física, Universidade de São Paulo, Caixa Postal 66318, 05315-970, São Paulo, SP, Brazil

Received June 20, 2003; E-mail: Peter.Bloechl@tu-clausthal.de

Abstract: Density functional calculations are presented to unravel the first steps of nitrogen fixation of nitrogenase. The individual steps leading from the resting state to nitrogen binding at the FeMo-cofactor with a central nitrogen ligand are characterized. The calculations indicate that the Fe−Mo cage opens as dinitrogen binds to the cluster. In the resting state, the central cage is overall neutral. Electrons and protons are transferred in an alternating manner. Upon dinitrogen binding, one protonated sulfur bridge is broken. An axial and a bridged binding mode of dinitrogen have been identified. Adsorption at the Mo site has been investigated but appears to be less favorable than binding at Fe sites.

Atmospheric N_2 is the main natural source of nitrogen, which makes up about 10% of the dry mass of biological matter. Nitrogenase, a bacterial enzyme, is able to convert atmospheric nitrogen into ammonia and thus to break the strongest chemical bond in nature.

Nitrogenase consists of two proteins, the Fe protein and the MoFe protein. The former supplies electrons, which drive the reaction, while the latter contains an $MoFe_7S_9N$ cluster as the proposed active site. Despite the fact that the crystal structure of nitrogenase has been unraveled more than 10 years ago,[1−3] the reaction mechanism still remains elusive to date.

A puzzling feature in the crystal structure of the FeMo-cofactor was the apparent presence of a cavity surrounded by six iron sites. Most previous ab initio calculations rested on the assumption that the cage is empty. Recent crystallographic studies,[4] however, identified the presence of a central ligand in the cavity, being a C, an O, or an N atom. ENDOR studies[5] suggest it to be nitrogen (Figure 1), which is also supported by theoretical investigations.[6,7]

The reaction consumes eight electrons and protons and produces at least one sacrificial hydrogen molecule.[8]

$$N_2 + 8H^+ + 8e^- \rightarrow 2NH_3 + H_2$$

Protons are provided by the solvent and electrons by the Fe protein. This electron transfer, which requires the proteins to dissociate and associate, is the rate-limiting factor for nitrogen fixation. Electrons are transferred to the cofactor at a rate of about 1 to 10 s^{-1}.[9]

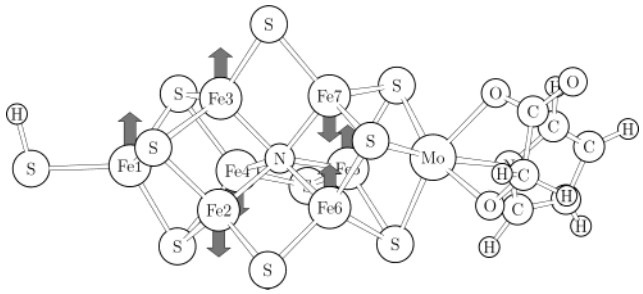

Figure 1. Resting state of the FeMo-cofactor.

A number of reaction mechanisms from nitrogen to ammonia at the FeMo-cofactor have been proposed. They can be classified according to the way N_2 binds to the cofactor: (1) Nitrogen binds head on to one of the six prismatic Fe atoms in an (η_1) coordination.[10−14] (2) Nitrogen forms an N_2 bridge between two octahedrally coordinated Fe atoms after opening of the cage,[15−17] and (3) N_2 coordinates to Mo.[18−22] (4) Binding of N_2 to the face formed by four Fe sites has been ruled out with the presence of a central ligand.[23]

[†] Clausthal University of Technology.
[‡] Universidade de São Paulo.

(1) Kim, J.; Rees, D. *Nature* **1992**, *360*, 553.
(2) Kim, J.; Rees, D. *Science* **1992**, *257*, 1667.
(3) Georgiadis, M.; Komiya, H.; Chakrabarti, P.; Woo, D.; Kornuc, J.; Rees, D. *Science* **1992**, *257*, 1653.
(4) Einsle, O.; Tezcan, F.; Andrade, S.; Schmid, B.; Yoshida, M.; Howard, J.; Rees, D. *Science* **2002**, *297*, 1696.
(5) Lee, H.; Benton, P.; Laryukhin, M.; Igarashi, R.; Dean, D.; Seefeldt, L.; Hoffman, B. *J. Am. Chem. Soc.* **2003**, *125*, 5604.
(6) Hinnemann, B.; Nørskov, J. *J. Am. Chem. Soc.* **2003**, *125*, 1466.
(7) Lovell, T.; Liu, T.; Case, D.; Noodleman, L. *J. Am. Chem. Soc.* **2003**, *125*, 8377.
(8) Burges, B.; Lowe, D. *Chem. Rev.* **1996**, *96*, 2983−3011.
(9) Fisher, K.; Newton, W.; Lowe, D. *Biochemistry* **2001**, *40*, 3333.
(10) Dance, I. *Chem. Commun.* **1997**, 165.
(11) Dance, I. *Chem. Commun.* **1998**, 523.
(12) Rod, T.; Hammer, B.; Nørskov, J. *Phys. Rev. Lett.* **1999**, *82*, 4054.
(13) Rod, T.; Nørskov, J. *J. Am. Chem. Soc.* **2000**, *122*, 12751−12763.
(14) Rod, T.; Logadottir, A.; Nørskov, J. *J. Chem. Phys.* **2000**, *112*, 5343−5347.
(15) Thorneley, R.; Lowe, D.; Dance, I.; Sellmann, D.; Sutter, J.; Coucouvanis, D.; Pickett, C. *JBIC, J. Biol. Inorg. Chem.* **1996**, *1*, 575−606.
(16) Sellmann, D.; Utz, J.; Blum, N.; Heinemann, F. *Coord. Chem. Rev.* **1999**, *190−192*, 607.
(17) Sellmann, D.; Fürsattel, A.; Sutter, J. *Coord. Chem. Rev.* **2000**, *200−202*, 545.
(18) Pickett, C. *J. Biol. Chem.* **1996**, *1*, 601.
(19) Grönberg, K.; Gormal, C.; Durrant, M.; Smith, B.; Henderson, R. *J. Am. Chem. Soc.* **1998**, *120*, 10613.
(20) Szilagyi, R.; Musaev, D.; Morokuma, K. *Inorg. Chem.* **2001**, *40*, 766.
(21) Durrant, M. *Biochemistry* **2002**, *41*, 13934.
(22) Durrant, M. *Biochemistry* **2002**, *41*, 13946.

10.1021/ja0367997 CCC: $25.00

Table 1. Core Configuration and Number of Projector Functions and Pairs of Partial Waves per Angular-Momentum State (l, m) with s-, p-, and d-character as Used in This Study

element	core	s	p	d
Fe(a)	[Ar]	2	2	2
Fe(b)	[Ne]	2	2	2
Mo(a)	[Kr]	3	3	2
Mo(b)	[Ar]$3d^{10}$	2	2	2
S	[Ne]	2	2	2
O	[He]	2	2	1
N	[He]	2	2	1
C	[He]	2	2	1
H	none	2	1	0

In this paper, we investigate the N_2 binding modes to the FeMo-cofactor using state-of-the-art electronic structure calculations. Particular emphasis is given to the identification of the oxidation and protonation state prior to N_2 binding in order to put the model assumption on a safe ground. We employ a more sophisticated description of the magnetic structure of the cluster than what has been possible in earlier work.

Inclusion of the central nitrogen ligand changes the reaction mechanism: The cage of the FeMo cluster opens up upon binding to nitrogen, supporting earlier suggestions that the cluster may undergo major rearrangements during the enzymatic cycle.[15] This indicates that the reaction mechanism is more complex than what has previously been believed. Moreover, we find that N_2 binds to the central cage, whereas binding to the Mo site, a major contender for the role as the reactive site of the cluster, is thermodynamically unstable.

1. Calculational Details

We performed first-principles electronic structure calculations based on density functional theory (DFT)[24,25] using the PBE functional.[26] Our choice has been motivated by the desire for a functional that is free of experimental parameters and that is widely distributed.

We employed the projector-augmented wave (PAW) method,[27,28] as implemented in the CP-PAW package, which describes the full wave functions without shape approximation. The PAW method decomposes the wave function into a plane wave part and two one-center expansions per atom. The plane wave part describes the wave functions properly outside the atomic regions, but within the covalent radius, it avoids the cusps and the nodal structure of the atoms. The true wave function and its plane wave counterpart are expanded at each atomic site into partial waves similar to atomic orbitals. To restore the correct behavior of the wave function near the nucleus, the difference between these one-center expansions are added to the plane wave part. Thus the full wave functions can be treated efficiently and accurately.

The parameters used for the augmentation are given in Table 1. The resting state has been investigated with setups Fe(a) and Mo(a), while the results with Fe(b) and Mo(b) have been reported for the N_2 binding modes. The maximum deviation between the N_2 binding energies calculated with (a) and (b) augmentations is 1.8 kJ/mol per metal atom. Freezing the semicore states (a) systematically increases the binding energy.

To isolate the molecules, the artificial electrostatic interaction between periodic images of the cluster in our plane-wave based method has been removed.[29] Wave function overlap has been avoided by keeping a distance of at least 6 Å between periodic images. We used a plane-wave cutoff of 30 Ry for the wave functions and 60 Ry for the density. This choice has been shown to be sufficient for a wide range of systems,[27] and the accuracy has been verified on smaller iron−sulfur clusters.

The FeMo-cofactor exhibits a complex spin structure with states that exhibit a noncollinear spin distribution. In conventional spin-polarized (spin-unrestricted) calculations, the spin distribution is forced to be uniaxial. Frustrated antiferromagnets such as the FeMo-cofactor on the other hand optimize the antiferromagnetic coupling by orienting the spin directions of different atoms at an angle. Therefore we implemented the option for noncollinear calculations[30−33] of the spin distribution into our PAW code. Such a description requires the wave functions to be two-component spinor functions $(\Psi_{n,\uparrow}(\vec{r}),\Psi_{n,\downarrow}(\vec{r}))$. The charge density ρ and local spin density $\vec{m}$ are then obtained as

$$\rho(\vec{r}) = -e\sum_n f_n[\Psi^*_{n,\uparrow}(\vec{r})\,\Psi_{n,\uparrow}(\vec{r}) + \Psi^*_{n,\downarrow}(\vec{r})\,\Psi_{n,\downarrow}(\vec{r})]$$

$$m_x(\vec{r}) = \frac{e\hbar}{2m_e}\sum_n f_n[\Psi^*_{n,\uparrow}(\vec{r})\,\Psi_{n,\downarrow}(\vec{r}) + \Psi^*_{n,\downarrow}(\vec{r})\,\Psi_{n,\uparrow}(\vec{r})]$$

$$m_y(\vec{r}) = -i\frac{e\hbar}{2m_e}\sum_n f_n[\Psi^*_{n,\uparrow}(\vec{r})\,\Psi_{n,\downarrow}(\vec{r}) - \Psi^*_{n,\downarrow}(\vec{r})\,\Psi_{n,\uparrow}(\vec{r})]$$

$$m_z(\vec{r}) = \frac{e\hbar}{2m_e}\sum_n f_n[\Psi^*_{n,\uparrow}(\vec{r})\,\Psi_{n,\uparrow}(\vec{r}) - \Psi^*_{n,\downarrow}(\vec{r})\,\Psi_{n,\downarrow}(\vec{r})]$$

where we used the nonrelativistic approximation for the g-factor $g_e = 2$. In our implementation, the exchange correlation potential is evaluated from the density and the absolute value of the magnetization as well as their gradients at each point. The resulting exchange-correlation potential has the form of a spatially varying magnetic field oriented parallel to the local magnetization.

An important technical advantage of a noncollinear calculation over a conventional collinear one is that it greatly simplifies the determination of the electronic ground state. The energy surface of a conventional calculation exhibits many metastable states, because every spin-flip requires an unfavorable transition state with a zero local spin. In a noncollinear description, the local spins can rotate without changing their magnitude, thus bypassing those barriers.

Except where explicitely mentioned, the spin ordering is optimized simultaneously with the atomic structure. This turned out to be important as the spin state depends strongly on the atomic configuration.

The Kohn−Sham Slater determinant of a noncollinear calculation is an eigenstate of neither S_z nor S^2, while that of a conventional calculation is an eigenstate of S_z. Within density functional theory, the physical quantity is the magnetization ($\vec{m}$). Therefore we evaluate the total spin as integral over the total magnetization.

$$\langle S^2\rangle = \hbar^2 S(S+1)$$

$$S = \frac{m_e}{e\hbar}\left|\int d^3r\,\vec{m}(\vec{r})\right|$$

We considered the complete FeMo-cofactor as shown in Figure 1. The central ligand has been chosen to be nitrogen. The ligands of the FeMo-cofactor have been truncated such that only single bonds were broken, and the open bonds were saturated by hydrogen atoms. Thus we included an imidazole and a glycolate coordinated to the Mo site to replace the histidine and homocitrate ligands, respectively, and an

(23) Dance, I. *Chem. Commun.* **2003**, *3*, 324.
(24) Hohenberg, P.; Kohn, W. *Phys. Rev. B* **1964**, *136*, 864.
(25) Kohn, W.; Sham, L. *Phys. Rev. A* **1965**, *140*, 1133.
(26) Perdew, J.; Burke, K.; Ernzerhof, M. *Phys. Rev. Lett.* **1996**, *77*, 3865.
(27) Blöchl, P. *Phys. Rev. B* **1994**, *50*, 17953.
(28) Blöchl, P.; Först, C.; Schimpl, J. *Bull. Mater. Sci.* **2003**, *26*, 33.
(29) Blöchl, P. *J. Chem. Phys.* **1986**, *103*, 7422.
(30) Sandratskii, L.; Guletskii, P. *J. Phys. F: Met. Phys.* **1986**, *16*, 43.
(31) Kübler, J.; Hock, K.-H.; Sticht, J.; Williams, A. *J. Phys. F: Met. Phys.* **1988**, *18*, 469.
(32) Oda, T.; Pasquarello, A.; Car, R. *Phys. Rev. Lett.* **1998**, *80*, 3622.
(33) Hobbs, D.; Kresse, G.; Hafner, J. *Phys. Rev. B* **2000**, *62*, 11556. Our approach differs from the implementation by Hobbs et al. in that we do allow for full noncollinearity also for the augmentation spin density.

SH group instead of a cysteine group at the terminal Fe atom of the cofactor.

Atomic structures have been optimized by damped Car−Parrinello[34] molecular dynamics with all degrees of freedom relaxed. The convergence has been tested by monitoring if the kinetic temperature remains below 5 K during a simulation of 0.05 ps (200 time steps). During that simulation, no friction has been applied to the atomic motion and the friction on the wave function dynamics has been chosen sufficiently low to avoid a noticeable effect on the atomic motion.

Transition states have been determined by applying a one-dimensional constraint on the atomic positions. In the present application, bond-length constraints have been used. The value of the bond length has been varied to maximize the energy, while all unconstrained degrees of freedom are allowed to relax to minimize the energy. Proof that this approach, when converged, determines exactly first-order transition states is given elsewhere.[35]

Interaction of the cofactor with the surrounding protein has been analyzed using a classical force field, namely the UFF force field.[36] The protein structure, as obtained from the protein data bank entry 1QGU,[37] has been included up to a radius of 15 Å and held rigid beyond a radius of 14 Å from the FeMoco center and relaxed inside. We excluded binding sites with an embedding energy greater than 200 kJ/mol relative to the resting state. This large tolerance has been chosen to account for uncertainties of the force field.

2. Resting State

Before exploring the N_2 binding, we need to determine the charge and protonation state of the cofactor. Since the driving forces for protonation and electron transfer are not known a priori, we derive them by comparing our theoretical results with experiment. This implies identifying the charge state of the resting state and to trace the electron- and proton-transfer steps until N_2 binds.

A reference is provided by the clear $S = {}^3/_2$ EPR signal[38] observed in the resting state. For the charge states with an odd electron number ranging from −2e to +4e, we find that only the charge state 0e, which is collinear, can be clearly identified with an $S = {}^3/_2$ spin state. In the definition of the charge state, we count the charge on the $MoFe_7S_9N$ subunit, while a charge of −3e is attributed to the ligands. Charges of +2e as well as +4e result in an $S = {}^1/_2$ state, and the charge state of −2e has a noncollinear spin distribution with $S = 0.24$. In our analysis, spin values may differ from half integer values as we deduce them from the magnetization as described previously. Full structural relaxation in each charge state has been important for the determination of the correct ground state as the spin distribution depends sensitively on the atomic structure. From this analysis, we conclude that the resting state is neutral, $[MoFe_7S_9N]^0$.

This spin arrangement is in agreement with the experimentally observed distribution of four sites aligned with the main spin direction and three antiparallel sites, as found in ENDOR[39,40] and Mössbauer[41] studies. Six Fe atoms form pairs with a parallel spin alignment. The pairs are antiferromagnetically coupled with the neighboring Fe sites as shown in Figure 1. One Fe atom, located next to the Mo site, remains unpaired and is antiferromagnetically coupled to all three of its Fe neighbors. Its spin is oriented in the minority spin direction.

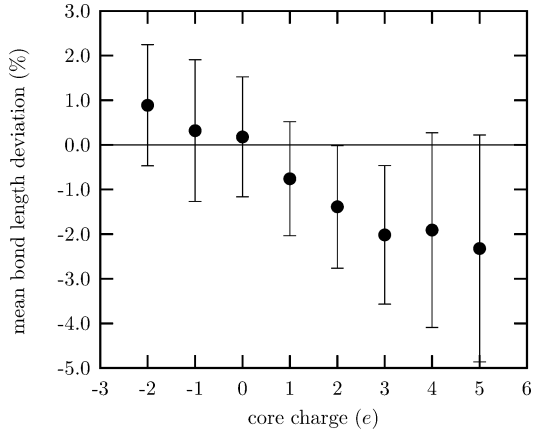

Figure 2. Change of the cluster size at different charges: The mean fractional deviation of calculated distances in various oxidation states relative to the X-ray structure.[4] All distances in $MoFe_7S_9N$ are considered. The error bars indicate the root-mean-square deviation from the mean value.

Table 2. Comparison of Experimental and Theoretical Bond Lengths (Å)[d]

	experiment				
	X-ray diffr.				
	2.0 Å[a]	1.6 Å[b]	1.16 Å[c]	EXAFS	theory
Mo−O	2.02	2.32	2.182	2.142	2.12
Mo−N	2.13	2.48	2.304	2.142	2.40
Mo−S	2.24	2.34	2.345	2.342	2.39
Mo−Fe	2.63	2.69	2.696	2.719	2.74
Mo−Fe′		5.06	5.062	5.060	5.10
Mo−Fe″	6.89	6.97	7.004		7.12
$Fe-S^3$	2.32	2.24	2.237	2.225	2.26
$Fe-S^2$	2.46	2.21	2.208	2.225	2.20
$Fe'-S^2$	2.46	2.23	2.221	2.225	2.20
$Fe'-S^1$	2.35	2.26	2.269	2.225	2.28
$Fe''-S^1$		2.28	2.268	2.225	2.28
Fe−Fe	2.52	2.65	2.622	2.612	2.60
Fe′-Fe′	2.59	2.68	2.657	2.612	2.63
Fe−Fe′	2.55	2.61	2.594	2.612	2.59
Fe−Fe′ d	3.60	3.73	3.700	3.660	3.68
Fe−N			2.003		1.99

[a] PDB 3MIN.[44] [b] 1QGU.[37] [c] 1M1N.[4] EXAFS distances refer to 45. Fe stands for the iron sites 5, 6, and 7; Fe′ stands for sites 2, 3, and 4; Fe″ stands for Fe1. S^3 are the sulfur sites connected to Mo; S^2 are the bridging sites; S^1 are those connected to Fe1. [d] Values shown are averaged over bonds related by the approximated three-fold symmetry.

The charge state derived from an analysis of the spin signal is consistent with that obtained by comparing the structures with X-ray diffraction data as shown in Figure 2. To compare the structures, we formed the mean fractional deviation of all interatomic distances within the cofactor. This quantity is a measure of the overall expansion of the cofactor. We find that the cluster expands nearly uniformly upon reduction, which is an indication for antibonding states being filled. The best agreement among the odd-electron states is obtained for the neutral cluster. Individual structural parameters are compared in Table 2. The atom coordinates are available as Supporting Information.

(34) Car, R.; Parrinello, M. *Phys. Rev. Lett.* **1985**, *55*, 2471.
(35) Blöchl, P.; Togni, A. *Organometallics* **1996**, *15*, 4125.
(36) Rappé A.; Casewit, C.; Colwell, K.; Goddard, W.; Skiff, W. *J. Am. Chem. Soc.* **1992**, *114*, 10024.
(37) Mayer, S.; Lawson, D.; Gormal, C.; Roe, S.; Smith, B. *J. Mol. Biol.* **1999**, *292*, 871.
(38) Münck, E.; Rhodes, H.; Orme-Johnson, W.; Davis, L.; Brill, W.; Shah, V. *Biochim. Biophys. Acta* **1975**, *400*, 32.
(39) Venters, R.; Nelson, M.; McLean, P.; True, A.; Levy, M.; Hoffman, B.; Orme-Johnson, W. *J. Am. Chem. Soc.* **1986**, *108*, 3487.
(40) True, A.; Nelson, M.; Venters, R.; Orme-Johnson, W.; Hoffmann, B. *J. Am. Chem. Soc.* **1988**, *110*, 1935.
(41) Yoo, S.; Angove, H.; Papaefthymiou, V.; Burgess, B.; Münck, E. *J. Am. Chem. Soc.* **2000**, *122*, 4926.

Our prediction of the charge state agrees with recent calculations using different functionals and methods,[7,23] which determined the charge state based on a comparison with measured redox potentials and mean Mössbauer isomer shifts.

Under the assumption that no central ligand is present, the comparison of experimental and theoretical results[42] lead to the prediction of a singly positive charged resting state $[MoFe_7S_9]^{1+}$. In the state $[MoFe_7S_9]^{1+}$ without central ligand, we obtain a noncollinear spin distribution. Including the central ligand, the analogous[43] oxidation state would be $[MoFe_7S_9N]^{2-}$ that is reduced by two electrons compared to the proposal of this work. Our spin ordering also differs from previous investigations,[6,7] which assumed it to be identical to their predictions without central ligand.[13,42]

In the neutral charge state, the formal charges can be assigned according to $Mo^{4.5+}(Fe^{2.5+})_5(Fe^{2+})_2(S^{2-})_9N^{3-}$, where the two Fe^{2+} cations are located next to the Mo site. While there is no unique procedure to determine formal charges, it is a useful concept for rationalizing the electronic structure. In the following, we will therefore analyze the chemical bonding in the cluster and thus rationalize our assignment.

The Fe sites are in a distorted tetrahedral environment formed by either four S ligands or three S ligands and the central N ligand, while the Mo site is octahedrally coordinated. The bonding network is augmented by metal−metal bonds, derived from the Fe e_g and Mo t_{2g} orbitals.

We analyzed the metal−metal bonds in a COOP-like analysis, by investigating the off-site density matrix elements corresponding to the σ-bond between the metal partners that are the d_{z^2} orbitals pointing toward each other. Atomic orbitals are defined in the PAW method via the partial wave expansion for each site. We observe a strong metal−metal bond character between the spin-paired Fe sites and between Mo and its Fe neighbors. We divided the electrons of these metal−metal bonds equally among the participating ions and added them to $Mo^{6+}(Fe^{3+})_7(S^{2-})_9N^{3-}$, which results in the assignment given above.

However, it should be noted that a weaker but nonzero bonding contribution is also found between antiferromagnetically coupled Fe sites. Those are not considered in the formal assignment, because formally the d-shell is filled in the majority spin direction of the participating atoms. Thus, metal−metal bonds connect the spin-paired Fe atoms and the Mo atom to its Fe neighbors.

Our assignment of formal charges accounts for the total charge and spin of the cluster. In addition, it explains the presence of a small magnetic moment of Mo antiparallel to the main spin direction.

3. Protonation of the Cofactor

To understand N_2 binding, one needs to determine the number of protons bound to the cofactor in the docking state.

To determine protonation of the cofactor, we investigated the protonation energies of all relevant proton acceptor sites for the singly reduced cofactor. After finding that the spin structure of the resting state is collinear, we calculated protonation energies by restricting the spin density to collinear configurations. In accordance with previous calculations without the central ligand,[13,46] we find that only the bridging sulfur atoms are protonated. Proton addition to the Fe atoms is less favorable by 19 kJ/mol and to the μ_3 sulfur atoms by 47 kJ/mol. A proton added to the Fe site converts into a hydride (H^-), which can react with a second proton to form a hydrogen molecule. The central ligand itself cannot directly be protonated.

The major protonation sites are hardly influenced by the inclusion of the central ligand, as seen from the comparison with previous studies.[13,46]

As obtained from collinear calculations, the protonation energy increases by approximately 250 kJ/mol per proton added to the sulfur bridges and decreases by the same amount for each electron added. This shows that a single proton is added to the cofactor for each additional electron in a ping-pong-like manner. Note that the dielectric screening by the environment affects the differences of the calculated protonation energies but not the qualitative finding of a ping-pong mechanism: The relative energies between different charge states are scaled down by a factor 3−5, assumed to be the dielectric constant of a protein.[47] The energies of any given charge state lie in a window 35 kJ/mol wide, which is less than the renormalized energy differences between different charge states.

Our results combined with experimental data provide us with the sequence of proton and electron-transfer steps. A reasonable assumption used in our analysis is that the proton-transfer rate is fast compared to the slow electron transfer.[48−51] This implies that the protonation state reaches thermal equilibrium before the next electron is transferred. The protonation state is then determined by the proton chemical potential reflecting the acidity of the cavity containing the cofactor. The proton chemical potential, not accessible in our calculation, will then be calibrated by comparing our findings with experiment.

The question if the resting state is protonated can be addressed by comparing our atomic structures with experiment. The main change upon protonation is a contraction of the mean bond length by 0.5%. The contraction is driven by the bond-angle reduction from 75° to 71° of a sulfur bridge upon proton addition. As the agreement of the unprotonated cluster structure with X-ray[4] and EXAFS[45,52] experiments is deteriorated by protonation, we conclude that the resting state is unprotonated. This fact provides us, when combined with the results depicted in Figure 3, with an upper bound for the proton chemical potential in the cavity.

A lower bound for the chemical potential is obtained from the observed structural changes after the first reduction step. EXAFS measurements indicate that the cluster contracts upon reduction by one electron for *Azotobacter vinelandii*,[52] while no significant changes have been found for *Klebsiella pneu-*

(42) Lovell, T.; Li, J.; Liu, T.; Case, D.; Noodleman, L. *J. Am. Chem. Soc.* **2001**, *123*, 12392.
(43) We consider as the analogous state one, which has the same formal oxidation number of the metal sites. The total charge of the two analogous states differ by −3e, the charge of the central ligand.
(44) Peters, J.; Stowell, M.; Michael, S.; Soltis, S.; Finnegan, M.; Johnson, M.; Rees, D. *Biochemistry* **1997**, *36*, 1181−1187.
(45) Harvey, I.; Strange, R.; Schneider, R.; Gormal, C.; Garner, C.; Hasnain, S.; Richards, R.; Smith, B. *Inorg. Chim. Acta* **1998**, *275*−*276*, 150−158.
(46) Lovell, T.; Li, J.; Case, D.; Noodleman, L. *J. Am. Chem. Soc.* **2002**, *124*, 4546.
(47) Lovell, T.; Li, J.; Case, D.; Noodleman, L. *J. Biol. Inorg. Chem.* **2002**, *7*, 735.
(48) Simpson, F.; Burris, R. *Science* **1984**, *224*, 1095.
(49) Thorneley, R.; Lowe, D. *Biochem. J.* **1984**, *224*, 887.
(50) Lowe, D.; Thorneley, R. *Biochem. J.* **1984**, *224*, 895.
(51) Thorneley, R.; Lowe, D. *Biochem. J.* **1984**, *224*, 903.
(52) Christiansen, J.; Tittsworth, R.; Hales, B.; Cramer, S. *J. Am. Chem. Soc.* **1995**, *117*, 10017.

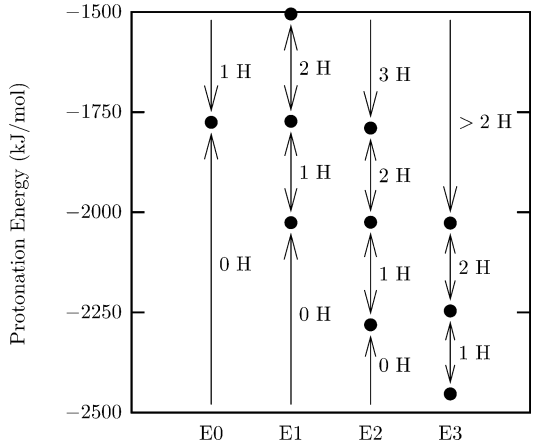

Figure 3. Protonation energies for different charge states of the cofactor. E_0 refers to the resting state, for which the cluster is charge neutral. E_1 to E_3 denote the states with 1−3 additional electrons.

moniae.[53] While electron transfer alone does not change the structure of the cofactor appreciably in our calculations, the protonation decreases the angle of the sulfur bridges, which in turn contracts the cluster. Thus the first reduction step causes the first proton to be transferred to one of the three sulfur bridges of the cofactor in *Azotobacter vinelandii*,[52] while no proton transfer takes place in *Klebsiella pneumoniae*.[53] The fact that proton transfer, as apparent by the contraction, depends on subtle changes of the protein between different bacteria's nitrogenases with the same functionality allows us to identify the proton chemical potential approximately with the first protonation energy of the cofactor reduced by one electron. Thus the protonation state can be determined for each charge state to within one proton.

$$E_0 \rightarrow E_1;\ E_1H_1 \rightarrow E_2H;\ E_2H_2 \rightarrow E_3H_2;\ E_3H_3$$

The notation E_xH_y describes a cofactor with *x* electrons and *y* protons added to the resting state. Semicolons separate different possible protonation states for each reduction step. Each arrow denotes one electron transfer.

4. N_2 Binding: Axial Coordination to Fe

We have investigated N_2 binding after transfer of one, two, and three electrons with the corresponding number of protons, that is, E_1H_1, E_2H_2, and E_3H_2. Our calculations indicate that N_2 binds only at E_2H_2 and E_3H_2, while the binding energy at E_1H_1 vanishes within our numerical accuracy. Our result that N_2 binds to the doubly protonated cofactor seems to disagree with the Thorneley−Lowe scheme[49−51] which predicts that 3−4 electrons reach the MoFe protein before N_2 binding. However, EPR measurements during turnover[9] indicate that only two of the three first electrons transferred to the protein actually reach the cofactor. Thus we need to add one electron (and one proton) before comparing our results for the cofactor with the Thorneley−Lowe scheme. If that is taken into account, our calculations are consistent with the predictions of Thorneley and Lowe.

On the basis of the doubly reduced cofactor, that is E_2H_2, we investigated several binding modes of N_2: (1) on the faces of the central cage, (2) in the bridging position between Mo and Fe, (3) at the Mo site, and at the Fe atoms of the central cage in (4) axial, (5) equatorial, and (6) side-on orientations. All of these complexes have been previously discussed and investigated theoretically for the complex without the central nitrogen ligand.

Table 3. Binding Energies and Reaction Barriers Concerning N_2 Binding[a]

binding site	barrier	binding energy
axial open	27	−19
axial closed		+12
bridged	66	−14
Mo		+30 to +33

[a] All energies are given in kJ/mol. Negative values indicate exothermic binding.

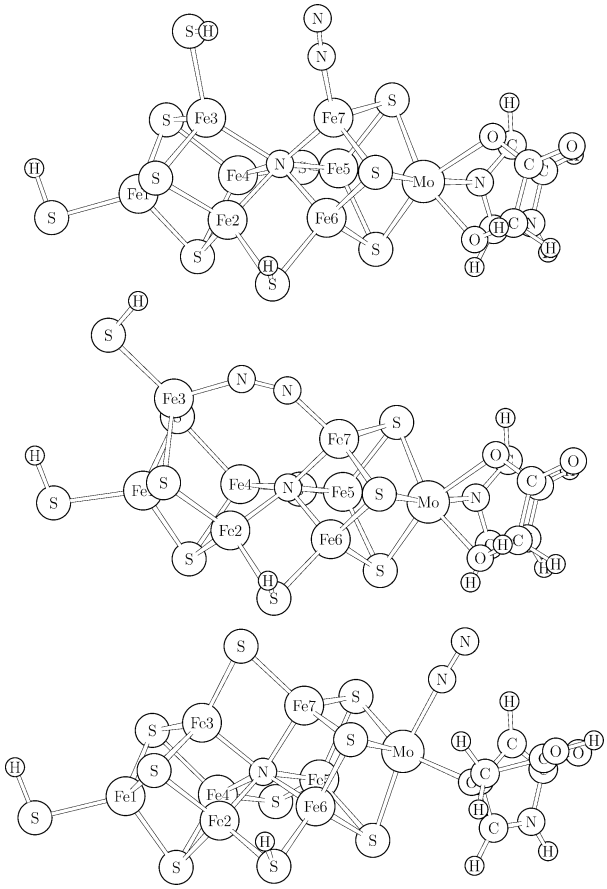

Figure 4. Structures of the three N_2 binding modes investigated in this work: the open axial mode (top), the bridged mode (middle), and Mo coordination (bottom).

According to our calculations, only binding to an Fe atom on the central cage is stable. All relevant energies are given in Table 3. Upon binding of N_2 to an Fe site next to a protonated sulfur bridge, we find that the sulfur bridge breaks so that the cage structure of the cofactor is disrupted. Binding and cage opening occur in a concerted mechanism. The resulting structure is shown in Figure 4. The barrier for N_2 binding is 27 kJ/mol, which can be overcome by thermal fluctuations. The binding energy is 19 kJ/mol.

Given the approximation of our methods, we cannot completely rule out binding at this point to be slightly endothermic. However, we find that the binding energy increases with the number of transferred electrons and protons. Thus even if

(53) Eady, R.; Smith, B.; Abraham, Z.; Dodd, F.; Grossmann, J.; Murphy, L.; Strange, R.; Hasnain, S. *Journal de physique* **1997**, *C2*, 611.

binding at this point is inefficient, the system will proceed to the next electron transfer and protonation step and bind there. We do not expect this to qualitatively affect our results.

For the cofactor without the central ligand, Rod et al.[12] found that N_2 binds in an axial mode to the same Fe site, but the cage structure of the cofactor remained intact in these calculations. We find that this result changes radically when the central nitrogen ligand is included. Compared to the metastable structure analogous to that of Rod et al., the cage opening stabilizes N_2 binding by 31 kJ/mol, indicating that N_2 does not bind unless the sulfur bridge breaks away. N_2 docking to the cofactor without opening of the cage is endothermic with 12 kJ/mol. The structure with a closed cage is metastable, with a small barrier < 10 kJ/mol toward the ground state.

One might have expected that the additional bonds to the central ligand result in a more rigid cofactor. Surprisingly the opposite is true, and the central ligand apparently leads to a more flexible structure of the cofactor. The reason for this behavior is that the number of bonds to the Fe sites is increased, which facilitates the dissociation of Fe ligands. As we will show below, the central ligand furthermore offers a variable number of bonds and thus lends additional flexibility to the cofactor.

With an N−H distance of 3.0 Å, the SH group seems to be well positioned for the first protonation of dinitrogen, which is believed to have the largest energy barrier in the catalytic cycle. However, according to our calculations, this proton transfer is energetically not favorable.

5. N_2 Binding: Bridged Coordination to Fe

The axial binding mode is not the only possible configuration for the N_2 complex with the FeMo-cofactor. We find that, in the axial mode, dinitrogen can tilt to form a dinitrogen bridge between the two Fe atoms formerly bridged by an SH group. As dinitrogen binds to the second Fe atom, the bond of this Fe atom to the central N ligand breaks in a concerted mechanism, so that the tetrahedral coordination of the Fe atom is recovered. This bridging configuration shown in Figure 4 is energetically less stable by 5 kJ/mol than the open axial mode; thus its binding energy is 14 kJ/mol. The reaction barrier of 66 kJ/mol corresponds to a reaction rate somewhat smaller than the electron transfer rate from the Fe protein to the MoFe protein. Thus both structures, with an axial and bridged dinitrogen, are equally likely intermediates for the N_2 fixation cycle.

A similar binding mode with N_2 bridging two Fe sites has been proposed earlier by Sellmann et al.[16] Sellmann's model differs from our bridged complex in that the Fe sites are octahedrally coordinated, while in our cluster the Fe atoms are tetrahedrally coordinated. The different coordination reflects in a major difference of the electronic structure: The octahedral complex results in low-spin Fe atoms while the tetrahedral coordination results in high-spin Fe atoms, which have different chemical behavior. The chemical analogy to octahedral low-spin complexes[54] has been one of the main motivations for Sellmann's proposal.

The additional ligands in Sellmann's model are water molecules and the nitrogen atoms from two amino acids of the protein, glutamine Glnα191 and histidine Hisα195.[55] We have investigated the model proposed by Sellmann by modeling the nitrogen ligands with ammonia molecules. We find this structure at least metastable in the absence of the central nitrogen ligand. Addition of the central ligand, however, results in the spontaneous desorption of the three water ligands from the two bridged Fe sites. The ammonia ligands remain bound to the Fe sites, so that the latter assume a pentacoordinate coordination with high-spin Fe atoms.

6. Embedding in the Protein Environment

An important question is if the protein environment is able to accommodate the expansion of the cage after N_2 binding. Therefore we embedded the rigid FeMo-cofactor as obtained from our calculations into the protein simulated with classical force fields.

The cofactor with N_2 adsorbed at sites Fe3 and Fe7 can easily be accommodated both in the axial and in the bridged configuration. These binding modes have the lowest embedding energies. Unless access to these sites is kinetically hindered, Fe3 and Fe7 are the preferred binding sites.

Szilagyi et al.[56] and Durrant[57] have investigated potential proton pathways from the surface to the cofactor and find a single path which can transfer protons from the inner surface of the protein toward homocitrate. Our own estimates confirm this finding. While Szilagyi et al. only considered crystalline water molecules, our investigation included also residues with flexible proton acceptor or donor sites and cavities that may contain noncrystalline water. We did not find any other proton paths from a cofactor molecule to the protein surface. This one path starts at various atoms at the inner surface between the two parts of the dimer and then leads via about 18 atoms (most of them water and two alcohol −OH groups of residues) to a water molecule near the cluster. This water molecule resides near Fe7 and is 3.7−4.0 Å away from the three sulfur neighbors around Fe7. Thus it is able to protonate the sulfur site bridging Fe7 and Fe3.

It is notable that the proton pathway directly leads to that region of the cofactor, which most easily accommodates N_2.

Mutagenesis studies,[58,59] in which Valα70 has been replaced by glycine conclude that the binding occurs at the face spanned by the iron sites 2, 3, 6, and 7. This is consistent with binding to Fe3 or Fe7 as predicted by our study.

We conclude that the adsorption complexes can be accommodated in the central cage. The most likely adsorption sites are Fe3 and Fe7.

7. N_2 Binding to the Mo Site

Coordination of N_2 to Mo has been discussed in great detail in the literature.[18−22] There is a large experimental effort to produce Mo-based model systems of nitrogenase. Recently such a system has been presented that reduces N_2 to NH_3 and that rivals natural MoFe-nitrogenase in efficiency.[60,61]

While the presence of the Mo atom in the cofactor stands out, it is not essential: there are other nitrogenases, where the Mo atom of the cofactor is replaced by V or Fe.[62,63]

(54) Sellmann, D.; Sutter, J. *J. Biol. Inorg. Chem.* **1996**, *1*, 597.
(55) Our notation refers to nitrogenase of *Azotobacter vinelandii*.
(56) Szilagyi, R.; Musaev, D.; Morokuma, K. *THEOCHEM* **2000**, *506*, 131.
(57) Durrant, M. *Biochem. J.* **2001**, *355*, 569.
(58) Mayer, S.; Niehaus, W.; Dean, D. *J. Chem. Soc., Dalton Trans.* **2002**, *5*, 802.
(59) Benton, P.; Laryukhin, M.; Mayer, S.; Hoffman, B.; Dean, D.; Seefeldt, L. *Biochemistry* **2003**, *42*, 9102.
(60) Yandulov, D.; Schrock, R. *Science* **2003**, *301*, 76−78.
(61) Leigh, G. *Science* **2003**, *301*, 55−56.
(62) Eady, R. *Chem. Rev.* **1996**, *96*, 3013−3030.

The Mo atom is octahedrally coordinated to three sulfur sites of the cofactor, to two oxygen atoms of homocitrate, and to the nitrogen atom of a histidine. N_2 association on the Mo atom is initiated by a proton transfer to the carboxyl group of homocitrate. After protonation, the Mo−O bond becomes very labile. Nevertheless, N_2 binding to the vacant coordination site at Mo is endothermic by 30−33 kJ/mol irrespective of the protonation state of the carboxyl group of homocitrate. The corresponding complex is metastable. While hydrophobic forces of the environment, not considered in this work, may increase the affinity to N_2, the presence of more stable binding modes at the Fe sites provides strong evidence that the mechanism does not proceed at the Mo site.

Our finding that binding of N_2 to Fe is exothermic is in agreement with earlier calculations.[10−14] We attribute disagreement with predictions in favor of binding to Mo[20,21] to the small cluster size, that is, 1−2 metal sites, used in those calculations.

8. Conclusion

In this work, we analyzed the N_2 binding at the FeMo-cofactor of nitrogenase containing the recently detected central nitrogen ligand by means of DFT calculations. The spin structure has been analyzed as a function of the oxidation state. Comparison with the experimental spin signal indicates that the charge state of the resting state is $[MoFe_7S_9N]^0$.

An investigation of the protonation cascade results in a ping-pong mechanism for electron and proton transfer. Protons attach to the bridging sulfur atoms. Molecular hydrogen is produced if protons add to an Fe site next to a protonated sulfur bridge. After at least two electrons and protons have been transferred to the resting state, dinitrogen binds to the cofactor.

Our calculations indicate that N_2 does not bind to the Mo site. We find that N_2 binds to an Fe site of the central cage. N_2 binding disrupts the cage of the FeMo-cofactor. In contrast to the obvious assumption that the central ligand adds rigidity to the cofactor, the additional nitrogen atom offers a variable number of bonds to its Fe neighbors and thus adds flexibility to the structure. One stable binding mode is head-on binding to one Fe site, which opens the protonated sulfur bridge. Opening of the sulfur bridge strengthens the nitrogen bond to the cofactor.

The complex can transform into a second structure where dinitrogen bridges the Fe sites formerly connected by a sulfur bridge. Both configurations are energetically nearly degenerate and transform substantially faster than the turnover rate. This transformation is facilitated by the presence of the central ligand.

Simple force field estimates of the embedding energy indicate that the most likely N_2 binding sites will be the iron atoms Fe3 and Fe7. An analysis of the proton transport channels confirms earlier results that predict only a single channel to the cavity holding the cofactor. The sites Fe3 and Fe7 are located next to this channel.

The observation of the significant role of the central ligand on the nitrogen binding provides new directions for the search of the mechanism of biological nitrogen fixation.

Acknowledgment. We acknowledge support by the HLRN for granting access to their IBM pSeries 690 supercomputers. This work has benefited from the collaboration within the ESF program on “Electronic Structure Calculations for Elucidating the Complex Atomistic Behaviour of Solids and Surfaces”. The TOC graphic has been prepared using Molden.[63]

Supporting Information Available: Calculational details (PDF). This material is available free of charge via the Internet at http://pubs.acs.org.

JA0367997

(63) Schaftenaar, G.; Noordik, J. *J. Comput.-Aided Mol. Des.* **2000**, *14*, 123.